ORIGINAL RESEARCH

Carotid Artery Stents: In Vitro Comparison of Different Stent Designs and Sizes Using CT Angiography and Contrast-Enhanced MR Angiography at 1.5T and 3T

M. Lettau
A. Sauer
S. Heiland
S. Rohde
M. Bendszus
S. Hähnel

BACKGROUND AND PURPOSE: CT angiography (CTA) and MR angiography (MRA) are increasingly used methods for evaluation of stented vessel segments. Our aim was to compare CTA, contrast-enhanced MRA (CE-MRA) at 1.5T, and CE-MRA at 3T for the visualization of carotid artery stents and to define the best noninvasive imaging technique as an alternative to conventional angiography for each stent.

MATERIALS AND METHODS: CTA and CE-MRA appearances of 18 carotid artery stents of different designs and sizes (4.0 to 10.0 mm) were investigated in vitro. For each stent, artificial lumen narrowing (ALN) was calculated.

RESULTS: With CE-MRA at 3T and at 1.5T, ALN in most nitinol stents was lower than that in the groups of stainless steel and cobalt alloy stents. In most nitinol stents and in both cobalt alloy stents, ALN was lower on CE-MRA at 3T than at 1.5T. In all stainless steel stents, ALN was lower on CTA than on CE-MRA. With CTA and CE-MRA, in most stents ALN decreased with increasing stent diameter.

CONCLUSIONS: CTA and CE-MRA evaluation of vessel patency after stent placement is possible but is considerably impaired by ALN. Investigators should be informed about the method of choice for every stent. Stent manufacturers should be aware of potential artifacts caused by their stents during noninvasive diagnostic methods such as CTA and CE-MRA.

Stent-protected angioplasty of the extracranial carotid artery has become a globally used and widely spread method for stroke prevention as an alternative to endarterectomy.[1] One major problem is the occurrence of in-stent neointimal growth, which can result in hemodynamically relevant restenosis or occlusion of the stented vessel segment (in-stent restenosis). The method of choice for the detection of restenosis within stented cervical vessel segments is intra-arterial conventional angiography, which can be associated with subsequent neurologic complications.[2] Especially because postinterventional Doppler sonography is often strongly dependent on the examiner's skills, CT angiography (CTA) or MR angiography (MRA) may help to decide whether residual stenoses or restenoses are evident. The aim of our study was to compare the appearance of carotid artery stents on CTA with the appearance on contrast-enhanced MR angiography (CE-MRA) at 1.5T and 3T. Of particular interest was the measurement of artificial lumen narrowing (ALN) caused by the stent material within the stented vessel segment to determine whether CTA or CE-MRA can be used to detect restenosis within the stent.

Materials and Methods

We examined a total of 18 stents (Table 1), which were deployed in silicon tubes (neoLab, Heidelberg, Germany) with different diameters (4.0–10.0 mm). The stented tubes were positioned in a plastic bowl filled with saline solution at 37°C to ensure complete expansion of the stents. Digital photographs and x-ray images (biplanar angiographic system; Integris, Philips Medical Systems, Best, the Netherlands; tube voltage = 80 kV; tube current = 1.5 mAs; diameter of the x-ray image amplifier = 17 cm; focus-film-distance = 90 cm) were taken of the stented tubes (Fig 1). The diameter (D_{xray}) of each stent after balloon inflation was calculated on the basis of a radiopaque reference scale that was simultaneously x-ray imaged with the stented tubes.

CTA

The stents were evaluated as follows: The phantom contained a solution of 0.9% sodium chloride (NaCl). Each stented tube was axially scanned after it was filled with diluted contrast medium (iomeprol, Imeron; Bracco-Byk Gulden, Konstanz, Germany). As described previously,[3] for this imaging, a 1-volume part of contrast medium was mixed with a 50-volume part of a solution of 0.9% NaCl, resulting in a fluid with a mean attenuation of 200 HU. All CT measurements were performed according to the same protocol (detector collimation, 2 × 0.5 mm; table feed per rotation, 1.2 mm; imaging matrix, 512 × 512; section thickness, 0.5 mm; FOV, 230 mm; tube voltage, 120 kV; tube current, 300 mAs; rotation time, 500 ms; convolution kernel, H40fS9C0). The in-plane pixel size was 0.449 × 0.449 mm^2.

CE-MRA

According to other published protocols,[4,5] before MR examination, the tubes were filled with 2.00 mmol/L of gadopentetate dimeglumine in saline solution: 1 L of saline solution was mixed with 4 mL of gadopentetate dimeglumine (0.5 mol/L; Magnevist; Bayer Schering Pharma, Berlin, Germany). CE-MRA was performed both at 1.5T (Magnetom Symphony; Siemens Medical Solutions, Forchheim, Germany) and at 3T (Magnetom Trio; Siemens Medical Solutions). The stented tubes were placed parallel to the z-axis of the MR imaging scanners; the scanning plane was generally coronal (meaning perpendicular to the y-axis of the scanners). The scanning protocol included a short 3D T1-weighted spoiled gradient-echo (T1 fast-field echo)

Received March 9, 2009; accepted after revision May 22.

From the Division of Neuroradiology, Department of Neurology, University of Heidelberg Medical Center, Heidelberg, Germany.

Please address correspondence to Michael Lettau, MD, Division of Neuroradiology, Department of Neurology, University of Heidelberg Medical Center, Im Neuenheimer Feld 400, D-69120 Heidelberg, Germany; e-mail: michael_lettau@gmx.de

DOI 10.3174/ajnr.A1743

Table 1: Properties of the analyzed stents

Stent/Tube Name	Acronym in This Article	Manufacturer	Material	Nominal Stent Diameter/Length (mm)	Tube Diameter (mm)	D_{xray} (mm)
Acculink	AC4	Guidant, Indianapolis, Ind	Nitinol	6/40	4	4.31
Acculink	AC5	Guidant	Nitinol	6/40	5	5.10
Dynalink	DY6	Guidant	Nitinol	7/56	6	5.99
Dynalink	DY7	Guidant	Nitinol	8/38	7	6.91
Dynalink	DY8	Guidant	Nitinol	9/56	8	7.92
Omnilink	OM5	Guidant	SS 316 L	5/18	5	5.38
Omnilink	OM6	Guidant	SS 316 L	6/18	6	5.10
Omnilink	OM7	Guidant	SS 316 L	7/38	7	6.66
Omnilink	OM8	Guidant	SS 316 L	8/58	8	7.28
Omnilink	OM9	Guidant	SS 316 L	9/18	9	8.56
Omnilink	OM10	Guidant	SS 316 L	10/18	10	9.20
Protegé	PRO	ev3, St. Paul, Minn	Nitinol	6/30	5	4.92
Carotid Wallstent	WAL7	Boston Scientific Ireland Galway, Ireland	Cobalt alloy	7/40	7	6.94
Carotid Wallstent	WAL9	Boston Scientific	Cobalt alloy	9/40	9	9.16
Xact	X6/8	Abbott Vascular Devices, Mervue, UK	Nitinol	6–8 mm*/40	7	6.61
Xact	X7	Abbott Vascular	Nitinol	8/30	7	7.09
Xact	X8	Abbott Vascular	Nitinol	9/30	8	7.90
Xact	X8/10	Abbott Vascular	Nitinol	8–10 mm*/30	9	8.42

Note:—D_{xray} indicates x-ray diameter; SS, stainless steel.
* Tapered stent.

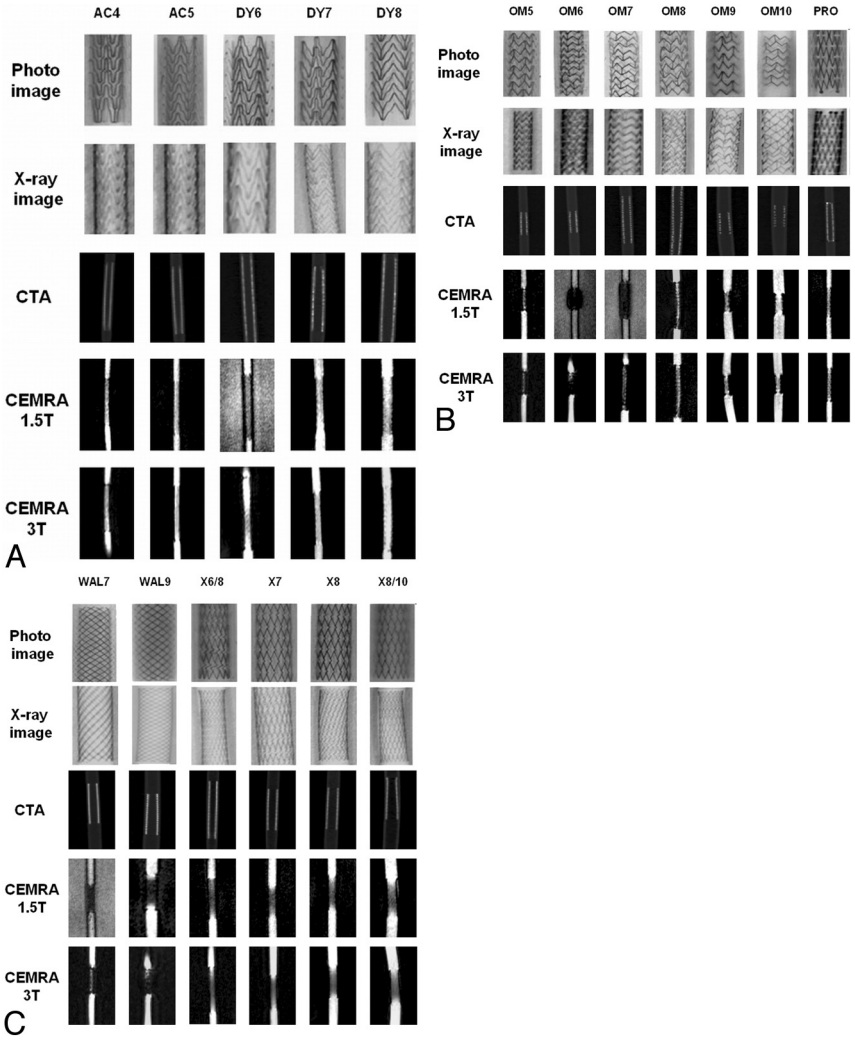

Fig 1. Imaging features of the stents. Stent acronyms are defined in Table 1. CTA indicates CT angiography; CEMRA, contrast-enhanced MR angiography.

Table 2: MR imaging parameters

Parameter	1.5T	3T
Sequence	3D T1 FFE	3D T1 FFE
Orientation	Perpendicular to tube wall	Perpendicular to tube wall
TR (ms)	3.66	4.5
TE (ms)	1.44	1.28
Flip angle (°)	30	30
Bandwidth (Hz/pixel)	430	430
Section thickness (mm)	0.8	0.8
Sections/partitions	80	60
FOV (mm)	300	300
Matrix	384	384
GRAPPA factor	2	2
Acquisition time (sec)	21	23

Note:—FFE indicates fast-field echo; GRAPPA, generalized autocalibrating partially parallel acquisition.

CE-MRA sequence at both field strengths (Table 2). The design of the CE-MRA sequences was guided by the following considerations: 1) the shortest TR possible to achieve maximal saturation of the extravascular tissues and to provide the best contrast-to-noise ratio, 2) the shortest TE possible to minimize signal-intensity loss due to dephasing, and 3) an FA of 30° as a compromise between short scanning time and optimized suppression of the static tissue.

Evaluation

With CTA and CE-MRA, the apparent stent diameter was measured by the visual inspection of 1 person (A.S.) after magnifying the images in 3 consecutive sections in the middle of the proximal, middle, and distal third of the stents along the x- and y-axes—that is, perpendicular to the tube wall—when the tubes were filled with diluted contrast medium by using defined window settings. From these 6 measurements, the mean value was calculated. On CTA, the mean stent diameter, as measured at a window width of 1500 HU and a window level of 400 HU, was defined as D_{CTA}. On CE-MRA, the mean stent diameter was defined as D_{CEMRA}. From these data, the ALN was calculated for each stent as follows: $ALN_{CTA} = [1 - (D_{CTA}/D_{xray})] \times 100\%$, and $ALN_{CEMRA} = [1 - (D_{CEMRA}/D_{xray})] \times 100\%$.

Reliability of the Measurements

All measurements were performed by 1 person (A.S.) who had been intensively trained in MRA and CTA measurements before the study by S.H., a senior neuroradiologist with personal experience in >10,000 CTA and MRA studies. Additionally, we calculated the intraclass correlation coefficients (Statistical Package for the Social Sciences reliability analysis; SPSS, Chicago, Ill) for inter- (A.S. versus S.H.) and intraobserver reliability of our measurements before, during, and after the study on 30 randomly chosen individual stent measurements.

Results

The strongest ALN was observed in the groups of stainless steel and cobalt-alloy stents on CE-MRA at 1.5T (Fig 2). The lowest ALN was detected in some nitinol stents on CE-MRA at 3T. With CE-MRA at 3T and at 1.5T, ALN in most nitinol stents was lower than that in the groups of stainless steel and cobalt alloy stents (Table 3). In most nitinol stents and in both cobalt alloy stents, ALN was lower on CE-MRA at 3T than at 1.5T. The strongest ALN at 1.5T among the group of nitinol stents was found in Xact stents (Abbott Vascular Devices, Mervue, UK). In most nitinol stents, ALN on CE-MRA at 3T was lower than that on CTA. In all stainless steel stents, ALN was lower on CTA than on CE-MRA. With CTA and CE-MRA, in most stents ALN decreased with increasing stent diameter.

Reliability of the Measurements

Intraclass correlation coefficients for inter- and intraobserver reliability of our measurements were >0.9 for all measurements, indicating an excellent intra- and interobserver agreement.

Discussion

Stent-protected angioplasty of the extracranial carotid artery has become a globally used and widespread method for the treatment of carotid artery stenoses.[1] Because intra-arterial conventional angiography, the method of choice for the detection of restenosis within stented cervical vessel segments, is limited by cost and patient hospitalization and can be associated with subsequent neurologic complications, CTA and MRA are increasingly used methods for evaluation of stented vessel segments.

To determine whether CTA can be used for the detection of restenosis within the stent, we evaluated the CT features of various stents that are suitable for carotid stent placement. Because vessel contrast in CTA is exclusively based on the difference between the attenuation of the vessel filled with contrast medium and the attenuation of the surrounding tissue and not on flow phenomena, our static phantom design is well suited to simulate CTA. Hähnel et al[3] found stronger ALN with a window width of 500 HU at a window level of 200 HU, which is the recommended standard window for CTA, compared with a window width of 1500 HU at a window level of 400 HU, as in other groups[6]; we preferred the latter window setting for the evaluation of stents with CTA. Heuschmid et al[7] found the image quality of medium and sharp image kernels on CTA to be good to fair, whereas a smooth kernel provided only acceptable-to-poor image quality; we used medium image kernels (H 40 f), as routinely used on CTA in our division. With CTA, artifacts such as exaggerated thickening or blooming of the stent struts, resulting in ALN of the stented tubes, are well known.

Our study showed markedly different degrees of ALN between 18.48% and 44.32% in vascular stents under simulated CTA conditions, most of them lower than the ALN that Hähnel et al[3] observed in small-vessel stents for intracranial angioplasty (2.0–4.0 mm) and Maintz et al[8] detected in coronary artery stents (2.5–5.0 mm) and stronger than the ALN Strotzer et al[6] observed in different stents with diameters from 8 to 10 mm. Hähnel et al[3] investigated small-vessel stents and observed stronger ALN in the group of 2.0-mm stents than in the groups of 3.0- and 4.0-mm stents. In our study, we also found a correlation between ALN and stent diameter, because in most stents, ALN decreased with increasing stent diameter. Because the strongest ALN was 44.32%, in-stent vessel stenoses of >44.32% should be detected with CTA and reliable evaluation of the stent lumen seems possible, because in our division, patients with in-stent restenoses are treated with balloon angioplasty if they present with clinical symptoms while receiving drug therapy and if their stenoses are ≥50% according to the North American Symptomatic Carotid Endarterectomy Trial criteria.[9]

When metallic stents are present, MR imaging artifacts caused by flow, susceptibility, and radio-frequency artifacts

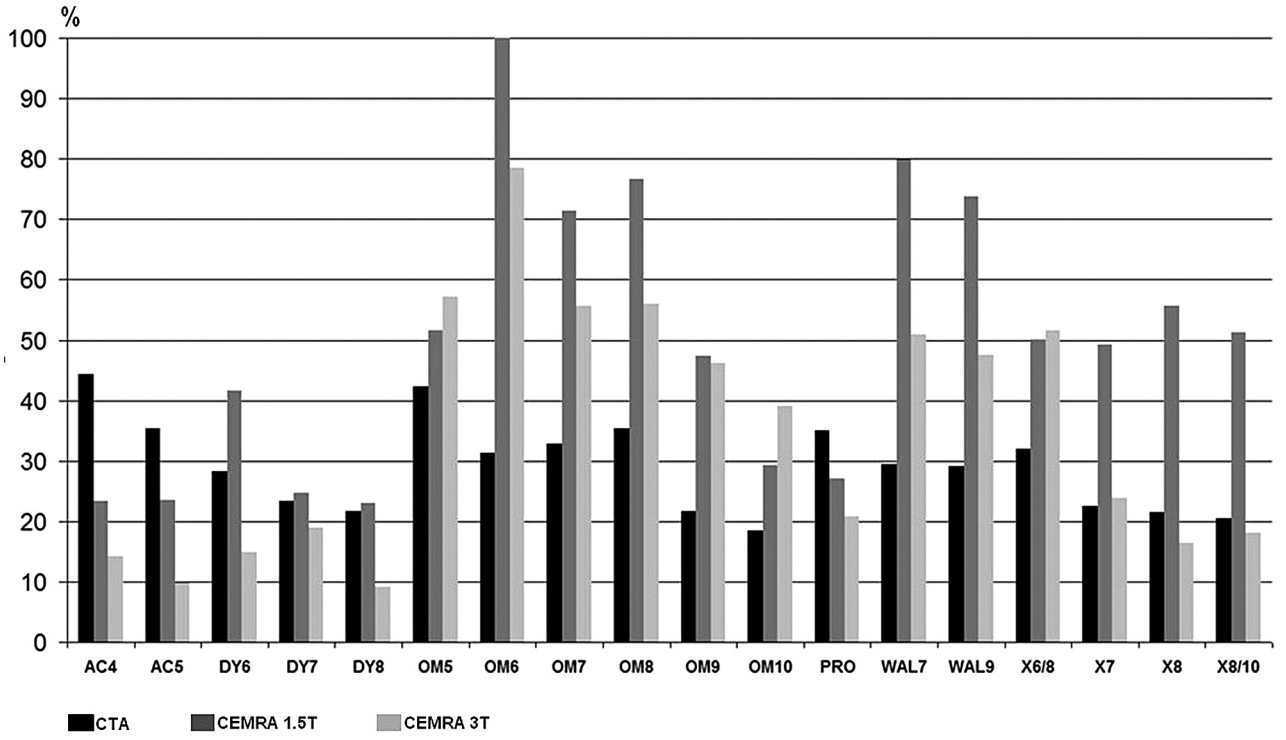

Fig 2. Artificial lumen narrowing of the stents on CTA and CE-MRA at 1.5T and 3T

Table 3: ALN (MV/SD) of the stents on CTA and CE-MRA at 1.5T and 3T

Stents	No.	CTA (MV/SD)	1.5T (MV/SD)	3T (MV/SD)
All stents	18	29.14/7.59	49.99/22.97	34.94/20.93
Nitinol	10	28.41/7.98	36.95/13.77	19.76/12.08
Stainless steel	6	30.35/8.86	65.68/24.40	54.85/13.34
Cobalt alloy	2	29.22/0.25	76.82/4.26	49.31/2.41

Note:—ALN indicates artificial lumen narrowing; CTA, CT angiography; CE-MRA, contrast-enhanced MR angiography; MV, mean value.

(eddy currents) may occur. Susceptibility artifacts result from local inhomogeneities of the magnetic field due to the metallic stent struts.[10] Besides the field strength of the MR imaging scanner, susceptibility artifacts depend on the magnetic susceptibility of the stent relative to the surrounding tissue and the blood within the vessel, on the orientation of the stent relative to the static magnetic field, and on the MR imaging parameters.[11] Whereas susceptibility artifacts are well understood and documented, radio-frequency artifacts are not. Bartels et al[12] explained the radio-frequency caging inside cagelike implants to be caused by disturbances of the send-and-receive sensitivities due to coupling between the loops in the implant and the send-and-receive coils of the MR imaging scanner. A scaled excitation angle model describing the behavior of the signal intensity inside the implants as a function of the applied nominal excitation angle was introduced. In the following time, Wang et al[13] performed a quantitative evaluation of susceptibility and radio-frequency artifacts of different stents.

The influence of the field strength of the MR imaging scanner on artifacts due to stents was evaluated by several groups. Klemm et al[14] and Graf et al[15] found stronger susceptibility artifacts at 1T compared with 0.2T, especially in stainless steel stents. Krämer et al[16] and Wall et al[5] described higher signal intensity–to-noise ratio (SNR) values within the stents at 3T compared with 1.5T, but the pattern of artifacts inside the stents evidently did not differ. Scanning at 1.5T and 3T, Hähnel et al[17] found the same ALN in most stents, but lower ALN at 3T compared with 1.5T in several nitinol and stainless steel stents. In most stents, we detected lower ALN at 3T than at 1.5T (Table 3). Stent material generally influences artifacts on MR imaging. Wang et al[13] quantitatively estimated susceptibility and radio-frequency artifacts at 1.5T and found susceptibility artifacts negligible (<1%) for non-stainless steel (nitinol, platinum, cobalt alloy) stents and totally destructive (100%) for the stainless steel stent. Signal-intensity loss due to radio-frequency artifacts was 31%–62% for nitinol stents, 14%–50% for platinum stents, 50%–77% for the cobalt alloy stents, and undetermined for the stainless steel stents. In our study, ALN in most nitinol stents was lower than that in the groups of stainless steel and cobalt alloy stents (Table 3). Buecker et al[18] developed a special MR imaging alloy consisting of >90% copper and demonstrated artifact-free visualization of the renal stent lumen at 1.5T.

MR image types and parameters generally influence artifacts on MR imaging. Performing MRA at 1.5T, several groups could demonstrate higher SNR inside stents at higher nominal excitation (flip) angles.[14,19-22] Using gradient-echo sequences at 0.2T and 1T, Klemm et al[14] found higher SNR inside stents with shorter TEs (4 ms compared with 10 ms). The radio-frequency (caging) artifacts inside metallic implants may be reduced by increasing the applied radio-frequency power in the excitation pulse. There is, however, a limit to the amount of radio-frequency energy that can safely be deposited in the body (specific absorption rate limit set by the US Food

and Drug Administration). At very high excitation angles, this limitation imposes the need for prolonged TRs, to keep the radio-frequency power deposition within the safety margins. We performed MRA sequences with the shortest possible TRs and TEs routinely used in our division (Table 2).

Stent diameter may influence artifacts on MRA. Hähnel et al[17] found lower ALN on CE-MRA at higher stent diameters in nitinol stents at 3T and in stainless steel stents at 1.5T and 3T. In our study, we found a correlation between ALN and stent diameter because ALN decreased with increasing stent diameter in all the different stents (except Omnilink, Guidant, Indianapolis, Ind) at 1.5T and 3T (Fig 2). Much of the decrease in ALN with stent diameter is certainly due to the proportionate nature of the ALN calculation. Provided that the absolute extent of artifacts remains the same for different stent diameters, the ALN will decrease with increasing stent size.

Generally, knowledge of the stent type is most important in choosing the right imaging technique for noninvasive evaluation. Maintz et al[23] found CTA superior to MRA at 1.5T in the detection of in-stent stenoses in most stents and inferior in only 1 tantalum stent. Amano et al[24] compared CTA and MRA at 1.5T in patients with iliac artery stents and reported CTA to be superior in stainless steel stents and MRA to be superior in tantalum stents. In our study, CTA was superior in all stainless steel and cobalt alloy stents. In most nitinol stents, MRA at 3T was superior to CTA (Table 3).

Our study was performed in vitro with a static phantom design; therefore, it has several limitations: First, the absence of flow and pulsatility in our phantom study may reduce the comparability of an in vivo situation. CE-MRA mainly depends on the T1 shortening effects of gadopentetate dimeglumine and is less sensitive to flow and motion,[25] compared with time-of-flight MRA. However, the small amount of motion of the metal stent itself, which invariably occurs in vivo, has probably more effect on the ALN of MR imaging measurements than of CT measurements. Second, we did not evaluate how the visibility of a vessel containing a stent is influenced by the background signal intensity in different tissues. Third, the stented tubes were placed parallel, and the scanning plane was generally perpendicular to the z-axis of the scanners. In oblique scanning orientations and in vessels with a curved shape or irregular walls, ALN might be even more pronounced than was observed in our study. Fourth, despite being an objective criterion for the comparison of the different stents, ALN is an arbitrary parameter that does not exactly reflect the dimensions of the evaluable diameter of the stents. Fifth, we performed CE-MRA sequences, which were routinely used in our division, not comparing MR images with different parameters. Sixth, we attached importance to the fact that our results are transferable to clinical practice. Therefore, the assessment of ALN has been performed subjectively by manual measurements directly on the MR imaging scanner software without any image postprocessing. In the alternative case of objective measurements on the basis of a pixel-by-pixel analysis as reported previously,[3,17] CTA and MRA would have been comparable, only difficult, because artifacts from the stents are hyperattenuated in CT (high pixel value), but hypointense in MRA (low pixel value). Seventh, we did not simulate in-stent stenoses. All these limitations preclude the possibility that our results can be transferred directly to imaging in humans.

Acknowledgment

We thank Robin Joyce Barrows for her support with language correction.

References

1. Eckstein HH, Ringleb P, Allenberg JR, et al. **Results of the Stent-Protected Angioplasty versus Carotid Endarterectomy (SPACE) study to treat symptomatic stenoses at 2 years: a multinational, prospective, randomised trial.** *Lancet Neurol* 2008;7:893–902
2. Bendszus M, Koltzenburg M, Burger R, et al. **Silent embolism in diagnostic cerebral angiography and neurointerventional procedures: a prospective study.** *Lancet* 1999;354:1594–97
3. Hähnel S, Trossbach M, Braun C, et al. **Small-vessel stents for intracranial angioplasty: in vitro comparison of different stent designs and sizes by using CT angiography.** *AJNR Am J Neuroradiol* 2003;24:1512–16
4. Lenhart M, Volk M, Manke C, et al. **Stent appearance at contrast-enhanced MR angiography: in vitro examination with 14 stents.** *Radiology* 2000;217:173–78
5. Wall A, Kugel H, Bachman R, et al. **3.0 T vs. 1.5 T MR angiography: in vitro comparison of intravascular stent artifacts.** *J Magn Reson Imaging* 2005;22:772–79
6. Strotzer M, Lenhart M, Butz B, et al. **Appearance of vascular stents in computed tomographic angiography: in vitro examination of 14 different stent types.** *Invest Radiol* 2001;36:652–58
7. Heuschmid M, Wiesinger B, Tepe G, et al. **Evaluation of various image reconstruction parameters in lower extremity stents using multidetector-row CT angiography: initial findings.** *Eur Radiol* 2007;17:265–71
8. Maintz D, Seifarth H, Raupach R, et al. **64-slice multidetector coronary CT angiography: in vitro evaluation of 68 different stents.** *Eur Radiol* 2006;16:818–26
9. Bladin CF, Alexandrova NA, Murphy J, et al. **The clinical value of methods to measure carotid stenosis.** *Int Angiol* 1996;15:295–99
10. Schenck JF. **The role of magnetic susceptibility in magnetic resonance imaging: MRI magnetic compatibility of the first and second kinds.** *Med Phys* 1996;23:815–50
11. Bakker CJ, Bhagwandien R, Moerland MA, et al. **Simulation of susceptibility artifacts in 2D and 3D Fourier transform spin-echo and gradient-echo magnetic resonance imaging.** *Magn Reson Imaging* 1994;12:767–74
12. Bartels LW, Bakker CJ, Viergever MA. **Improved lumen visualization in metallic vascular implants by reducing RF artifacts.** *Magn Reson Med* 2002;47:171–80
13. Wang Y, Truong TN, Yen C, et al. **Quantitative evaluation of susceptibility and shielding effects of nitinol, platinum, cobalt-alloy, and stainless steel stents.** *Magn Reson Med* 2003;49:972–76
14. Klemm T, Duda S, Machann J, et al. **MR imaging in the presence of vascular stents: a systematic assessment of artifacts for various stent orientations, sequence types, and field strengths.** *J Magn Reson Imaging* 2000;12:606–15
15. Graf H, Klemm T, Lauer UA, et al. **Systematics of imaging artifacts in MRT caused by metallic vascular implants (stents)** [in German]. *Röfo* 2003;175:1711–19
16. Krämer SC, Wall A, Maintz D, et al. **3.0 Tesla magnetic resonance angiography of endovascular aortic stent grafts: phantom measurements in comparison with 1.5 Tesla.** *Invest Radiol* 2004;39:413–17
17. Hähnel S, Nguyen-Trong TH, Rohde S, et al. **3.0 Tesla contrast-enhanced MR angiography of carotid artery stents: in vitro measurements as compared with 1.5 Tesla.** *J Neuroradiol* 2006;33:75–80
18. Buecker A, Spuentrup E, Ruebben A, et al. **Artifact-free in-stent lumen visualization by standard magnetic resonance angiography using a new metallic magnetic resonance imaging stent.** *Circulation* 2002;105:1772–75
19. Bartels LW, Smits HF, Bakker CJ, et al. **MR imaging of vascular stents: effects of susceptibility, flow, and radiofrequency eddy currents.** *J Vasc Interv Radiol* 2001;12:365–71
20. Holton A, Walsh E, Anayiotos A, et al. **Comparative MRI compatibility of 316 L stainless steel alloy and nickel-titanium alloy stents.** *J Cardiovasc Magn Reson* 2002;4:423–30
21. Meyer JM, Buecker A, Spuentrup E, et al. **Improved in-stent magnetic resonance angiography with high flip angle excitation.** *Invest Radiol* 2001;36:677–81
22. Straube T, Wolf S, Flesser A, et al. **MRI of carotid stents: influence of stent properties and sequence parameters on visualization of the carotid artery lumen** [in German]. *Röfo* 2005;177:375–80
23. Maintz D, Tombach B, Juergens KU, et al. **Revealing in-stent stenoses of the iliac arteries: comparison of multidetector CT with MR angiography and digital radiographic angiography in a Phantom model.** *AJR Am J Roentgenol* 2002;179:1319–22
24. Amano Y, Ishihara M, Hayashi H, et al. **Metallic artifacts of coronary and iliac arteries stents in MR angiography and contrast-enhanced CT.** *Clin Imaging* 1999;23:85–89
25. Prince MR. **Gadolinium-enhanced MR aortography.** *Radiology* 1994;191:155–64